



Smoothed MHD equations for numerical simulations of ideal quasi-neutral gas dynamic flows

Mikhail V. Popov^{a,b,*}, Tatiana G. Elizarova^b

^a *École Normale Supérieure de Lyon, CRAL (UMR CNRS 5574), Université de Lyon 1, 46 allée d'Italie 69007 Lyon, France*

^b *Keldysh Institute of Applied Mathematics, 4, Miusskaya sq., Moscow, 125047, Russia*

ARTICLE INFO

Article history:

Received 9 September 2014

Received in revised form

6 July 2015

Accepted 9 July 2015

Available online 17 July 2015

Keywords:

Ideal magnetohydrodynamics

Conservative form

Quasi-gasdynamics equations

Finite-difference schemes

ABSTRACT

We introduce a mathematical model and related numerical method for numerical modeling of ideal magnetohydrodynamic (MHD) gas flows as an extension of previously known quasi-gasdynamics (QGD) equations. This approach is based on smoothing, or averaging of the original MHD equation system over a small time interval that leads to a new equation system, named quasi-MHD, or QMHD system. The QMHD equations are closely related to the original MHD system except for additional strongly non-linear dissipative τ -terms with a small parameter τ as a factor. The τ -terms depend on the solution itself and decrease in regions with the small space gradients of the solution. In this sense the QMHD system could be regarded as an approach with adaptive artificial dissipation. The QMHD is a generalization of regularized (or quasi-) gas dynamic equation system suggested in last three decades. In the QMHD numerical method the evolution of all physical variables is presented in a non-split divergence form. Divergence-free evolution of the magnetic field provides by using a constrained transport method based on Faraday's law of induction. Accuracy and convergence of the QMHD method is verified on a wide set of standard MHD tests including the 3D Orszag–Tang vortex flow.

© 2015 Elsevier B.V. All rights reserved.

1. Introduction

A variety of numerical methods to solve magnetohydrodynamic (MHD) equations have been developed. We mention some of them here—for example, the MacCormack scheme [1], the Lax–Friedrichs scheme [2], the weighted essentially nonoscillatory scheme [3], the piecewise parabolic method (PPM) [4], and its local variant PPM on a local stencil (PPML) [5,6]. All of them are equipped with limiter functions for suppressing oscillations near discontinuities and approximate Riemann solvers (e.g., the Roe solver [7], the Harten–Lax–van Leer contact solver [8], or the Harten–Lax–van Leer discontinuities solver [9]). For practical applications a number of numerical codes have been developed—for example, for astrophysical simulations, Flash [10], Enzo [11], Athena [12], and Castro [13].

An alternative model for numerical modeling of ideal quasi-neutral gas dynamic flows with subsonic and supersonic velocities under the action of an electromagnetic field is presented here. This

* Corresponding author at: École Normale Supérieure de Lyon, CRAL (UMR CNRS 5574), Université de Lyon 1, 46 allée d'Italie 69007 Lyon, France.

E-mail address: mikhail.v.popov@gmail.com (M.V. Popov).

model is based on smoothing, or averaging, of the original MHD equation system over a small time interval that leads to a new equation system, named a quasi-MHD (QMHD) system. From the physical point of view, the time-smoothing looks natural, taking into account that in physical experiments any measurements of gas dynamic quantities need some nonzero time interval. The QMHD system obtained here can be regarded as an extension of the quasi-gas dynamic (QGD) equation system suggested and studied in the last three decades for nonconducting gas flows [14–16].

The first version of the QGD equations was built in 1982 on the basis of a simple kinetic model, which describes the motion of particles as a cyclic process consisting of collisionless expansion and instantaneous relaxation to the Maxwell equilibrium. The finite-difference schemes obtained were oriented at the simulation of supersonic ideal gas flows. The corresponding differential representation of the finite-difference equations obtained were named the QGD system. Later the QGD system was derived phenomenologically without use of kinetic models [17]. The entropy theorem for the QGD system was established, and a family of new numerical algorithms based on central-difference approximations of the QGD system were suggested. QGD equations and associated numerical schemes were used as a basis for further development of the QGD approach for different gas dynamic problems. In particular, the QGD algorithms were built to describe viscous flows, weakly

compressible and incompressible fluids, free surface flows in the shallow water approximation, and MHD flows. We skip the full list of publications here because it is too long, and we direct the reader to three books, where all the main progress in QGD theory is collected [14–16].

The QGD equations are closely related to the Navier–Stokes equation system, and can be written in the form of the Navier–Stokes system except for additional strongly nonlinear terms. These additional terms contain the second-order space derivatives in a factor of a small parameter τ that has the dimension of time. These τ -terms bring an additional nonnegative entropy production that proves their dissipative character [15,16]. The last feature is a critical point for the mathematical description and numerical methods in fluid dynamics. The τ -terms depend on the solution itself, and decrease in regions where space derivatives of the solution are small. In this sense, being applied for the numerical simulations, the QGD system could be regarded as an approach with a special kind of adaptive artificial dissipation.

A family of finite-difference homogeneous schemes based on QGD equations was constructed. Efficiency, accuracy, and simplicity of the constructed algorithms are achieved by regularization by τ -terms, which are included in all equations of the system. The QGD schemes are constructed by application of a central-difference approximation for all space derivatives, where τ -terms contribute to the stability of the numerical solution.

The applicability of the QGD algorithm was demonstrated in [18], for example, where stability and accuracy are studied numerically for 10 classical Riemann test problems. The results revealed that the numerical solution monotonically converges to a self-similar one as the spatial grid is refined. Application of QGD algorithm for complex multidimensional gas dynamic problems can be found in [19–22], for example. The QGD algorithms are well suited for unstructured computational grids [15,23], and are quite naturally generalized for the parallel realization with the domain decomposition technique in order to speed up computation; see, for example, [14,15].

The advantages and disadvantages of the QGD approach for simulation of gas flows are both related to the τ -terms present in the equations. τ -terms have a stabilizing effect, which allows one to construct simple numerical algorithms. The possibility to tune the τ parameter allows one to simulate inviscid flows, where τ -terms are related to space discretization; viscous and rarefied flows, where τ -terms are related to the free path length; turbulent flows, where τ -terms play a role in subgrid dissipation. The important advantage of the QGD approach is the possibility to simulate a wide range of flows on the basis of the similar numerical algorithms.

The disadvantage of the QGD approach is the awkwardness of the equations compared with the Navier–Stokes-like systems. When τ -terms are computed on the basis of the space discretization, the QGD algorithm has only first-order space accuracy, which in some cases requires more finely spaced grids compared with the higher-order methods.

It is difficult to define the domain of applicability of QGD equations in comparison with Navier–Stokes equations. As the QGD system is closely related to the Navier–Stokes equation system, both systems have a number of common exact solutions. It was shown that τ -terms in QGD equations have the order of τ^2 for stationary flows. So the advantages of the QGD approach should be searched for in simulations of the rarefied flows, where τ -terms are not small, and for strongly nonstationary (turbulent) flows. In particular, it was shown that QGD equations allow one to describe rarefied gas dynamic flows with larger Knudsen numbers compared with Navier–Stokes equations [15,24]. The successful application of QGD equations for direct numerical simulation of the laminar–turbulent transition in subsonic gas flows is presented

in [25]. Another problem that was solved only in the framework of the QGD approach is the simulation of strongly underexpanded jet flow [26].

The mathematically important property of parabolicity of QGD equations for the general equation of state was proved in [27]. In the same article, an equation for entropy balance was obtained in the case of absence of heat sources. The heat source was considered in a later article [28], where the entropy balance equation was reformulated and some simulations of real gases were performed. Correctness of the Cauchy problem for QGD equations and its local solvability were proved [29]. Linearized stability of equilibrium solutions was proved in [30]. The latter contains a mathematically strict investigation which reveals the dissipativity of QGD equations and the smoothing properties.

The first variants of the QMHD equations were obtained in 1997 (e.g., [16]), where contrary to the present article, the magnetic field is taken as an action of an external force without time smoothing. The entropy theorem for the QMHD system was proved and examples of analytical solutions for the QMHD system were obtained for flows in a plane horizontal (Hartman flow) and a vertical channel. For both cases, the analytical solutions of QMHD equations converge to MHD solution as τ goes to zero. QMHD numerical calculations of an electrically conductive liquid melt in an external magnetic field were done in, for example, [31].

In the present article, in the same way as the QGD system was obtained as an extension of the Navier–Stokes equation system, the QMHD system is obtained on the basis of averaging of the original MHD system over a small time interval and taking into account gas viscosity and thermal conductivity. Averaging over time is done for all physical parameters, including the magnetic field. The first results for 1D and 2D MHD calculations were published in [32] and [33], respectively.

During the long history of development and application of the QGD approach presented, the assumption of negligibility of second-order time derivatives, which appear as a result of the averaging procedure, in comparison with the first-order ones, was always taken as a matter of course. In this article, this assumption is checked numerically for the first time.

In Section 2 the development of the QMHD system of equations is presented. The numerical algorithm and the finite-difference scheme are described in Section 3. The solenoidal condition for a magnetic field is presented in Section 4. Extensive testing of the QMHD scheme is discussed in Sections 5 and 6, including correct computation for complex cases of interaction with discontinuity of the tangential component of the magnetic field in 1D flows and a propagation of MHD waves in a 2D formulation. The Orszag–Tang vortex problem and the blast wave propagation test are discussed in Section 7. In conclusion, we discuss the possibilities of the QMHD scheme for other flow simulations.

2. QMHD system of equations

The system of MHD equations for a viscous thermally conductive gas with zero electrical resistivity can be written in the following form:

$$\frac{\partial \rho}{\partial t} + \frac{\partial \rho u_\alpha}{\partial x_\alpha} = 0, \quad (1)$$

$$\frac{\partial \rho u_\beta}{\partial t} + \frac{\partial T_{\alpha\beta}}{\partial x_\alpha} = 0, \quad (2)$$

$$\frac{\partial E}{\partial t} + \frac{\partial Q_\alpha}{\partial x_\alpha} = 0, \quad (3)$$

$$\frac{\partial B_\beta}{\partial t} + \frac{\partial T_{\alpha\beta}^m}{\partial x_\alpha} = 0, \quad (4)$$

where the indices denote coordinate axes $\alpha, \beta = x, y, z$,

$$\begin{aligned} T_{\alpha\beta} &= \rho u_\alpha u_\beta + p \delta_{\alpha\beta} - \Pi_{\alpha\beta} + \frac{1}{2} B^2 \delta_{\alpha\beta} - B_\alpha B_\beta, \\ Q_\alpha &= \rho u_\alpha H - \Pi_{\alpha\beta} u_\beta - q_\alpha + \frac{1}{2} u_\alpha B^2 - B_\alpha (u_\beta B_\beta), \\ T_{\alpha\beta}^m &= u_\beta B_\alpha - u_\alpha B_\beta, \\ E &= \rho \varepsilon + \frac{\rho u^2}{2} + \frac{B^2}{2}, \quad H = \frac{E + p}{\rho} \\ u^2 &= u_x^2 + u_y^2 + u_z^2, \quad B^2 = B_x^2 + B_y^2 + B_z^2. \end{aligned} \tag{5}$$

Here ρ is the density, u_α are the velocity components, B_α are the components of magnetic field, E and H are the total energy per unit volume and total specific enthalpy, respectively, p is the pressure, and ε is the specific internal energy. The term $\sqrt{1/4\pi}$ is included in the definition of B . The system (1)–(3) is supplemented by an equation of state, which in the case of an ideal gas, has the form

$$p = (\gamma - 1) \rho \varepsilon,$$

where γ is the adiabatic index.

The viscous stress tensor and the heat-flux vector are defined as follows:

$$\begin{aligned} \Pi_{\alpha\beta} &= \mu \left\{ \frac{\partial u_\alpha}{\partial x_\beta} + \frac{\partial u_\beta}{\partial x_\alpha} - \frac{2}{3} \delta_{\alpha\beta} \left(\frac{\partial u_x}{\partial x} + \frac{\partial u_y}{\partial y} + \frac{\partial u_z}{\partial z} \right) \right\}, \\ q_\alpha &= -k \frac{\partial T}{\partial x_\alpha}, \end{aligned}$$

where μ is the dynamic viscosity coefficient,

$$k = \frac{\mu \gamma R}{(\gamma - 1) Pr}$$

is the heat transfer coefficient, R is the universal gas constant, and Pr stands for the Prandtl number.

Using the same approach as in [34], we average the system (1)–(4) over a small time interval δt and calculate the time integrals approximately as

$$\frac{1}{\delta t} \int_t^{t+\delta t} f(x_\alpha, t') dt' \approx f(x_\alpha, t) + \tau \frac{\partial f(x_\alpha, t)}{\partial t},$$

where f denotes the averaging quantities. We assume that δt is smaller than the characteristic hydrodynamic time and that all averaged values practically do not depend on the time interval δt in some range of δt [15, 16]. τ is small and related to an interval of time averaging ($0 \leq \tau \leq \delta t$), that is not strictly determined. So τ may be considered as a free small parameter that will be defined later.

Then the system (1)–(4) can be rewritten as

$$\begin{aligned} \frac{\partial}{\partial t} \left(\rho + \tau \frac{\partial \rho}{\partial t} \right) + \frac{\partial}{\partial x_\alpha} \left(\rho u_\alpha + \tau \frac{\partial \rho u_\alpha}{\partial t} \right) &= 0, \\ \frac{\partial}{\partial t} \left(\rho u_\beta + \tau \frac{\partial \rho u_\beta}{\partial t} \right) + \frac{\partial}{\partial x_\alpha} \left(T_{\alpha\beta} + \tau \frac{\partial T_{\alpha\beta}}{\partial t} \right) &= 0, \\ \frac{\partial}{\partial t} \left(E + \tau \frac{\partial E}{\partial t} \right) + \frac{\partial}{\partial x_\alpha} \left(Q_\alpha + \tau \frac{\partial Q_\alpha}{\partial t} \right) &= 0, \\ \frac{\partial}{\partial t} \left(B_\beta + \tau \frac{\partial B_\beta}{\partial t} \right) + \frac{\partial}{\partial x_\alpha} \left(T_{\alpha\beta}^m + \tau \frac{\partial T_{\alpha\beta}^m}{\partial t} \right) &= 0. \end{aligned}$$

Analogously to development of the QGD system, we drop all second-order time derivatives, supposing they are small compared with the first-order time derivatives:

$$\left| \frac{\partial}{\partial t} \tau \frac{\partial f}{\partial t} \right| \ll \left| \frac{\partial f}{\partial t} \right|, \tag{6}$$

where f is a considered variable. For example, the continuity equation under assumption (6) is

$$\frac{\partial \rho}{\partial t} + \frac{\partial}{\partial x_\alpha} \left(\rho u_\alpha + \tau \frac{\partial \rho u_\alpha}{\partial t} \right) = 0.$$

We define the time derivative of momentum from the equation of motion:

$$\frac{\partial \rho u_\alpha}{\partial t} = - \frac{\partial}{\partial x_\beta} \left(\rho u_\alpha u_\beta + p \delta_{\alpha\beta} + \frac{1}{2} B^2 \delta_{\alpha\beta} - B_\alpha B_\beta \right),$$

where we restrict our consideration to first-order terms only—that is, we omit terms of the order of $O(\tau \mu)$ and switch indices $\alpha \leftrightarrow \beta$. Introducing the definitions

$$\begin{aligned} w_\alpha &= \frac{\tau}{\rho} \frac{\partial}{\partial x_\beta} \left(\rho u_\alpha u_\beta + p \delta_{\alpha\beta} + \frac{1}{2} B^2 \delta_{\alpha\beta} - B_\alpha B_\beta \right), \\ J_\alpha &= \rho (u_\alpha - w_\alpha), \end{aligned} \tag{7}$$

we present the continuity equation in smoothed form as follows:

$$\frac{\partial \rho}{\partial t} + \frac{\partial J_\alpha}{\partial x_\alpha} = 0. \tag{8}$$

In the same way, omitting the terms of order $O(\tau k)$, we write the other equations of the QMHD system as

$$\frac{\partial \rho u_\beta}{\partial t} + \frac{\partial T_{\alpha\beta}^n}{\partial x_\alpha} = \frac{\partial \Pi_{\alpha\beta}^n}{\partial x_\alpha}, \tag{9}$$

$$\frac{\partial E}{\partial t} + \frac{\partial F_\alpha}{\partial x_\alpha} + \frac{\partial Q_\alpha^n}{\partial x_\alpha} = \frac{\partial \Pi_{\alpha\beta}^n u_\beta}{\partial x_\alpha}, \tag{10}$$

$$\frac{\partial B_\beta}{\partial t} + \frac{\partial T_{\alpha\beta}^m}{\partial x_\alpha} = - \frac{\partial T_{\alpha\beta}^{mn}}{\partial x_\alpha}, \tag{11}$$

where

$$F_\alpha = J_\alpha \left(H + \frac{B^2}{2\rho} \right) - B_\alpha (u_\beta B_\beta),$$

$$T_{\alpha\beta}^n = J_\alpha u_\beta + p \delta_{\alpha\beta} + \frac{1}{2} B^2 \delta_{\alpha\beta} - B_\alpha B_\beta,$$

$$\Pi_{\alpha\beta}^n = \Pi_{\alpha\beta} - \rho u_\alpha \Delta u_\beta - \Delta p \delta_{\alpha\beta} - \frac{1}{2} (\Delta B)^2 \delta_{\alpha\beta} + \Delta (B_\alpha B_\beta),$$

$$\begin{aligned} Q_\alpha^n &= -q_\alpha + \rho u_\alpha \Delta \varepsilon + \rho u_\alpha (p + B^2) \Delta \frac{1}{\rho} \\ &\quad + u_\alpha (B_\beta \Delta B_\beta) - B_\alpha (B_\beta \Delta u_\beta), \end{aligned}$$

$$T_{\alpha\beta}^{mn} = \Delta u_\beta B_\alpha - \Delta u_\alpha B_\beta + u_\beta \Delta B_\alpha - u_\alpha \Delta B_\beta, \tag{12}$$

with τ -terms presented with use of the definition $\tau \partial f / \partial t = \Delta f$. Here Δ -terms are defined from the known MHD equations:

$$\Delta \frac{1}{\rho} = -\tau \left(u_\alpha \frac{\partial}{\partial x_\alpha} \frac{1}{\rho} - \frac{1}{\rho} \frac{\partial u_\alpha}{\partial x_\alpha} \right), \tag{13}$$

$$\Delta u_\alpha = -\tau \left(u_\beta \frac{\partial u_\alpha}{\partial x_\beta} + \frac{1}{\rho} \frac{\partial p}{\partial x_\alpha} + \frac{1}{\rho} \frac{\partial}{\partial x_\beta} \frac{B^2}{2} \delta_{\alpha\beta} - \frac{1}{\rho} \frac{\partial B_\alpha B_\beta}{\partial x_\beta} \right), \tag{14}$$

$$\Delta \varepsilon = -\tau \left(u_\alpha \frac{\partial \varepsilon}{\partial x_\alpha} + \frac{p}{\rho} \frac{\partial u_\alpha}{\partial x_\alpha} \right), \tag{15}$$

$$\Delta p = -\tau \left(u_\alpha \frac{\partial p}{\partial x_\alpha} + \gamma p \frac{\partial u_\alpha}{\partial x_\alpha} \right), \tag{16}$$

$$\Delta B_\alpha = \tau \frac{\partial}{\partial x_\beta} (u_\alpha B_\beta - u_\beta B_\alpha). \tag{17}$$

$$\Delta (B_\alpha B_\beta) = B_\alpha \Delta B_\beta + B_\beta \Delta B_\alpha. \tag{18}$$

The system (8)–(11) is the approximation of the initial system (1)–(4) with the order of τ , and for $\tau = 0$ equation system (8)–(11) reduces to the classical system (1)–(4). Notice that the averaging procedure and the introduction of the τ -terms do not disturb the solenoidal condition for the magnetic field $\text{div}\mathbf{B} = 0$. This property of QMHD equations was proved analytically in [35].

The original MHD equation system includes viscous and heat-conductive terms, but does not include the terms responsible for magnetic diffusivity. Magnetic diffusivity $\nu_m = c^2/(4\pi\sigma)$ (where σ is the electric conductivity) can be included in (added to) the right-hand side of (4) in the form

$$\nu_m \nabla (\mathbf{B} \times [\nabla \times \mathbf{B}]) = \nu_m \frac{\partial}{\partial x_\alpha} \left\{ B_\beta \left(\frac{\partial B_\beta}{\partial x_\alpha} - \frac{\partial B_\alpha}{\partial x_\beta} \right) \right\}, \quad (19)$$

which represents Joule heating, and the right-hand side of (3) in the form

$$\nu_m \frac{\partial^2 B_\alpha}{\partial x_\beta \partial x_\beta}. \quad (20)$$

So these terms appear on the right-hand side of (10) and (11) of the QMHD system in the form of (20) and (19) correspondingly. Below the effect of magnetic diffusivity is not taken into consideration.

Generalization of the QMHD system for a nonideal gas was performed in [35], including the influence of external forces and the heat source. This variant of the QMHD equations has the following form:

$$\frac{\partial}{\partial t} \rho + \text{div}[\rho(\mathbf{u} - \mathbf{w})] = 0, \quad (21)$$

$$\begin{aligned} \frac{\partial}{\partial t} (\rho \mathbf{u}) + \text{div}[\rho(\mathbf{u} - \mathbf{w}) \otimes \mathbf{u} - \mathbf{B} \otimes \mathbf{B}] + \nabla (p + \frac{1}{2} |\mathbf{B}|^2) \\ = \text{div} \Pi^n + [\rho - \tau \text{div}(\rho \mathbf{u})] \mathbf{F}, \end{aligned} \quad (22)$$

$$\begin{aligned} \frac{\partial}{\partial t} (E + \frac{1}{2} |\mathbf{B}|^2) + \text{div}[(E + p)(\mathbf{u} - \mathbf{w}) \\ + |\mathbf{B}|^2(\mathbf{u} - \widehat{\mathbf{w}}) - ((\mathbf{u} - \widehat{\mathbf{w}}) \cdot \mathbf{B}) \mathbf{B}] \\ = \text{div}[-\mathbf{q} + \tau(\boldsymbol{\beta} \cdot \mathbf{B}) \mathbf{u} + \Pi^n \mathbf{u}] + \rho(\mathbf{u} - \mathbf{w}) \cdot \mathbf{F} + Q_h, \end{aligned} \quad (23)$$

$$\begin{aligned} \frac{\partial}{\partial t} \mathbf{B} + \text{div}[(\mathbf{u} - \widehat{\mathbf{w}}) \otimes \mathbf{B} - \mathbf{B} \otimes (\mathbf{u} - \widehat{\mathbf{w}})] \\ = \text{div}[\tau(\mathbf{u} \otimes \boldsymbol{\beta} - \boldsymbol{\beta} \otimes \mathbf{u})], \end{aligned} \quad (24)$$

$$\text{div} \mathbf{B} = 0. \quad (25)$$

Here the operators div and ∇ are taken with respect to the spatial variables (x_1, x_2, x_3) . The divergence of a tensor is taken with respect to its first index. The signs \otimes and \cdot denote the tensor and inner products of vectors. The given functions $\mathbf{F} = \mathbf{F}(x, t)$ and $Q_h = Q_h(x, t) \geq 0$ represent the density of the body forces and the power of the heat sources. The auxiliary velocity vector functions \mathbf{w} and $\widehat{\mathbf{w}}$ are given by

$$\mathbf{w} = \frac{\tau}{\rho} [\text{div}(\rho \mathbf{u} \otimes \mathbf{u} - \mathbf{B} \otimes \mathbf{B}) + \nabla (p + \frac{1}{2} |\mathbf{B}|^2) - \rho \mathbf{F}],$$

$$\widehat{\mathbf{w}} = \frac{\tau}{\rho} [\rho(\mathbf{u} \nabla) \mathbf{u} - \text{div}(\mathbf{B} \otimes \mathbf{B}) + \nabla (p + \frac{1}{2} |\mathbf{B}|^2) - \rho \mathbf{F}].$$

The nonsymmetric regularized viscous stress tensor is written in the form

$$\begin{aligned} \Pi^n = \Pi + \rho \mathbf{u} \otimes \widehat{\mathbf{w}} - \tau(\boldsymbol{\beta} \otimes \mathbf{B} + \mathbf{B} \otimes \boldsymbol{\beta}) \\ + \tau \left(\mathbf{u} \nabla p + \rho C_s^2 \text{div} \mathbf{u} + \boldsymbol{\beta} \cdot \mathbf{B} - \frac{p_\Gamma}{\rho \varepsilon_\Gamma} Q \right) \mathbb{I}, \end{aligned}$$

where \mathbb{I} is the identity tensor, and C_s is the sound speed defined by

$$C_s^2 = p_\rho + \frac{T p_\Gamma^2}{\rho^2 \varepsilon_\Gamma}.$$

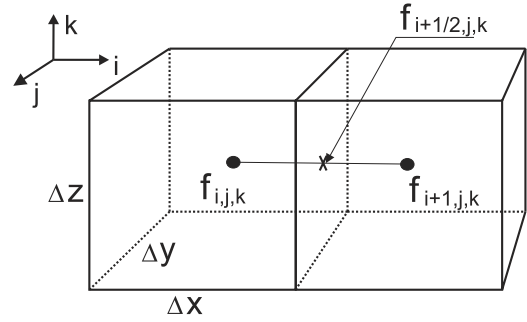


Fig. 1. Two adjacent cells with the set variables.

The regularized heat flux \mathbf{q} is given by

$$-\mathbf{q} = k \nabla T + \tau \left[\rho (\mathbf{u} \nabla \varepsilon - \frac{p}{\rho^2} \mathbf{u} \nabla \rho) - Q \right] \mathbf{u},$$

and the auxiliary vector function $\boldsymbol{\beta}$ has the form

$$\boldsymbol{\beta} = \text{div}(\mathbf{u} \otimes \mathbf{B} - \mathbf{B} \otimes \mathbf{u}).$$

QMHD system (21)–(25) is more compact and convenient for analytical analysis. It was used to study entropy properties of regularized equations and to derive the entropy balance equation [35]. This form might also allow a more straightforward finite-difference approximation because of its compactness and appropriate introduction of the $\boldsymbol{\beta}$ function. In the following, we use the index form (8)–(11).

3. Numerical algorithm

To construct the numerical algorithm, an explicit finite-difference scheme with central approximation of the space derivatives is used. A uniform grid is applied dividing the computational domain into cells of size $\Delta x \times \Delta y \times \Delta z$. Here Δ denotes the corresponding spatial step. Independent variables are assigned to the centers of the cells and are denoted by integer indices i, j, k , corresponding to the directions along the axes x, y, z . Half-integer indices denote the values on the interfaces between the cells. Fig. 1 shows two adjacent cells with the variables defined at their centers and on the interface between them.

In discretization of (8)–(11), approximation of first-order and second-order space derivatives is performed with half-integer nodes of the grid. As follows from Fig. 1, the derivatives are replaced by expressions as

$$\frac{\partial f}{\partial x} \Big|_{i,j,k} \rightarrow \frac{f_{i+1/2,j,k} - f_{i-1/2,j,k}}{\Delta x}, \quad (26)$$

$$\begin{aligned} \frac{\partial}{\partial x} \left(\xi \frac{\partial f}{\partial x} \right) \Big|_{i,j,k} \\ \rightarrow \frac{1}{\Delta x} \left(\xi_{i+1/2,j,k} \frac{\partial f}{\partial x} \Big|_{i+1/2,j,k} - \xi_{i-1/2,j,k} \frac{\partial f}{\partial x} \Big|_{i-1/2,j,k} \right), \end{aligned} \quad (27)$$

where

$$\frac{\partial f}{\partial x} \Big|_{i+1/2,j,k} \rightarrow \frac{f_{i+1,j,k} - f_{i,j,k}}{\Delta x},$$

where f denotes known values at time t , and ξ is an appropriate factor. For mixed derivatives we suggest the following approximation, which is successfully proved by simulations:

$$\begin{aligned} \frac{\partial}{\partial x} \left(\xi \frac{\partial f}{\partial y} \right) \Big|_{i,j,k} \\ \rightarrow \frac{1}{\Delta x} \left(\xi_{i+1/2,j,k} \frac{\partial f}{\partial y} \Big|_{i+1/2,j,k} - \xi_{i-1/2,j,k} \frac{\partial f}{\partial y} \Big|_{i-1/2,j,k} \right), \end{aligned} \quad (28)$$

where

$$\left. \frac{\partial f}{\partial y} \right|_{i+1/2,j,k} \rightarrow \frac{f_{i+1/2,j+1/2,k} - f_{i+1/2,j-1/2,k}}{\Delta y},$$

$$f_{i+1/2,j+1/2,k} = \frac{1}{2} (f_{i+1/2,j,k} + f_{i+1/2,j+1,k}),$$

$$f_{i+1/2,j,k} = \frac{1}{2} (f_{i,j,k} + f_{i+1,j,k}).$$

For time derivatives the expression is

$$\frac{\partial f}{\partial t} \rightarrow \frac{\hat{f}_{i,j,k} - f_{i,j,k}}{\Delta t}, \tag{29}$$

where Δt is a time step, and \hat{f} denotes unknown values at a new time point $t + \Delta t$. Rules (26)–(29) mean that the unknown values at a new time point are computed via the known values at the previous time point and the differences between the fluxes through the edges of the cell (i, j, k) .

All the required values $f_{i+1/2,j,k}$ and $\xi_{i+1/2,j,k}$ in (26)–(28) are computed from “primitive” variables $(\rho, u_x, u_y, u_z, B_x, B_y, B_z, p)$, which in turn are averaged between adjacent cells—for example, for the density we have

$$\rho_{i+1/2,j,k} = 0.5 (\rho_{i,j,k} + \rho_{i+1,j,k}),$$

and for total energy the equation of state is

$$E_{i+1/2,j,k} = \frac{p_{i+1/2,j,k}}{\gamma - 1} + \frac{1}{2} \{ \rho_{i+1/2,j,k} (u_{x i+1/2,j,k}^2 + u_{y i+1/2,j,k}^2 + u_{z i+1/2,j,k}^2) + B_{x i+1/2,j,k}^2 + B_{y i+1/2,j,k}^2 + B_{z i+1/2,j,k}^2 \}.$$

We arrive at an explicit time-difference scheme of the following form: for the density,

$$\hat{\rho}_{i,j,k} = \rho_{i,j,k} - \frac{\Delta t}{\Delta x} (J_{i+1/2,j,k} - J_{i-1/2,j,k}) - \frac{\Delta t}{\Delta y} (J_{i,j+1/2,k} - J_{i,j-1/2,k}) - \frac{\Delta t}{\Delta z} (J_{i,j,k+1/2} - J_{i,j,k-1/2}),$$

for the momentum components,

$$\begin{aligned} \widehat{\rho u}_{\beta i,j,k} &= \rho u_{\beta i,j,k} - \frac{\Delta t}{\Delta x} (T_{x\beta i+1/2,j,k}^n - T_{x\beta i-1/2,j,k}^n) \\ &\quad - \frac{\Delta t}{\Delta y} (T_{y\beta i,j+1/2,k}^n - T_{y\beta i,j-1/2,k}^n) \\ &\quad - \frac{\Delta t}{\Delta z} (T_{z\beta i,j,k+1/2}^n - T_{z\beta i,j,k-1/2}^n) \\ &\quad + \frac{\Delta t}{\Delta x} (\Pi_{x\beta i+1/2,j,k}^n - \Pi_{x\beta i-1/2,j,k}^n) \\ &\quad + \frac{\Delta t}{\Delta y} (\Pi_{y\beta i,j+1/2,k}^n - \Pi_{y\beta i,j-1/2,k}^n) \\ &\quad + \frac{\Delta t}{\Delta z} (\Pi_{z\beta i,j,k+1/2}^n - \Pi_{z\beta i,j,k-1/2}^n), \end{aligned}$$

and for the total energy,

$$\begin{aligned} \hat{E}_{i,j,k} &= E_{i,j,k} - \frac{\Delta t}{\Delta x} (W_{xi+1/2,j,k} - W_{xi-1/2,j,k}) \\ &\quad - \frac{\Delta t}{\Delta y} (W_{yi,j+1/2,k} - W_{yi,j-1/2,k}) \\ &\quad - \frac{\Delta t}{\Delta z} (W_{zi,j,k+1/2} - W_{zi,j,k-1/2}), \end{aligned}$$

where

$$W_{xi\pm 1/2,j,k} = F_{xi\pm 1/2,j,k} + Q_{xi\pm 1/2,j,k} \Pi_{x\beta}^n u_{\beta i\pm 1/2,j,k}, \quad \text{etc.}$$

The discretized form of (6) for a magnetic field will be described in the next section. The stencil for 3D flow computations consists of 27 space points.

Time step Δt is determined by the Courant condition:

$$\Delta t = C \cdot \min \left(\frac{\Delta x}{\max_{i,j,k} (|u_{xi,j,k}| + c_{fx i,j,k})}, \frac{\Delta y}{\max_{i,j,k} (|u_{yi,j,k}| + c_{fy i,j,k})}, \frac{\Delta z}{\max_{i,j,k} (|u_{zi,j,k}| + c_{fz i,j,k})} \right),$$

where C is the numerical Courant coefficient, and in computations it falls in the range 0.1–0.3 in most cases, and c_f is the fast magnetosonic velocity [36].

To determine the dissipative coefficients τ, μ , and k , we follow the QGD method where for viscous heat-conducting nonmagnetized flows τ is determined according to the kinetic theory as the Maxwell relaxation time $\tau = \lambda/c$ (λ is the mean free path, c is the sound velocity), and μ and k are related to τ as [37]

$$\mu = \tau \cdot p \cdot Sc, \quad k = \tau p \frac{Sc}{Pr} \frac{\gamma R}{\gamma - 1}, \tag{30}$$

where Sc is the Schmidt number. For QGD calculations of gas flows in the Euler approximation, where physical viscosity and heat conductivity coefficients are neglected, in the definition of τ we replace λ with the numerical space step h and determine $\tau = \alpha h/c$, where α is a tuning numerical coefficient, $0 < \alpha < 1$. In this way all dissipative coefficients are regarded as artificial regularization factors.

The same kinetic theory approach could be used for the QMHD system for MHD single-fluid quasi-neutral gas flows. In spite of the fact that plasmas have at least two particle species, in a single-fluid approximation the mean free paths of all interacting species are assumed to be similar, which determines a single Maxwell relaxation time. Otherwise the physics is essentially multifluid.

We solve system (8)–(11) in the Euler approximation and all dissipative terms, containing τ, μ , and k coefficients, are regarded as artificial regularization factors. Instead of sound velocity c , we determine τ using the fast magnetosonic velocity c_f .

$$\tau = \alpha \frac{h}{c_f}. \tag{31}$$

Since there are three fast magnetosonic velocities c_{fx}, c_{fy} , and c_{fz} , we should compute three different parameters τ_x, τ_y , and τ_z use them in (13)–(18) depending on the interface of the cell which we consider. In the same way, $h = \Delta x, \Delta y$ or Δz :

$$\tau_x = \alpha \frac{\Delta x}{c_{fx}}, \quad \tau_y = \alpha \frac{\Delta y}{c_{fy}}, \quad \tau_z = \alpha \frac{\Delta z}{c_{fz}}.$$

The use of c_{fx}, c_{fy} , and c_{fz} is necessary in magnetohydrodynamics, as the fastest perturbations in the presence of magnetic fields propagate with fast magnetosonic velocity, which has different values in different directions with respect to the local vector of the magnetic field. In practice, we put c_{fx}, c_{fy} , and c_{fz} as factors before the corresponding x, y , or z derivative.

For QGD and QMHD methods, α appears as the main tuning parameter (e.g., [15,23]). Theoretical investigations and practical experience show that for $\alpha \sim 1$, the numerical dissipation is increased and shock-wave fronts are smoothed. For $\alpha \lesssim 0.1$, numerical oscillations appear that may even destroy the numerical solution. So for practical applications, α can be taken in the range

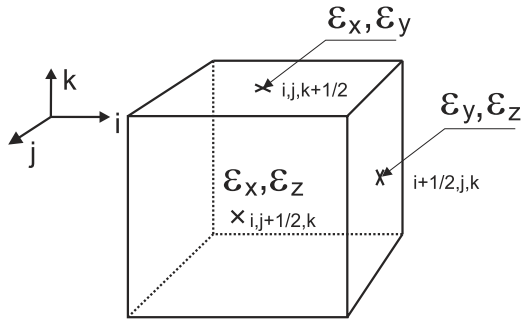


Fig. 2. The components of the electric field used in the equations for the magnetic field of the QMHD system.

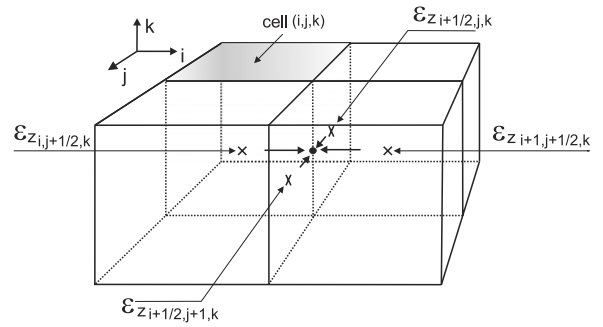


Fig. 3. Transport of the components of the electric field from the face centers to the edge centers.

between 0.1 and 0.5, depending on the problem considered and according to the accuracy and stability of the numerical algorithm. With base values $\alpha = 0.5$ and $Sc = Pr = 1$, the QGD and QMHD algorithms allow one to obtain a stable numerical solution for a large variety of gas dynamic flows, but the numerical viscosity introduced by the scheme is much higher normally than the physical viscosity present in a real system. This must be taken into account, but this is a common issue for all numerical methods.

In special cases the additional tuning of numerical coefficients Sc and Pr improves a numerical solution compared with the base results [18]. The influence of Sc on the numerical solution of MHD problems is demonstrated below in test case 6.2. For the other problems considered, Pr and Sc are chosen to be 1.

In the above numerical scheme all space derivatives are approximated by central differences, which provide accuracy of order $O(h^2)$. The definition of τ (31) decreases the accuracy down to $O(h)$, but allows the use of (30) with $\alpha = 0.5$, $Sc = 1$, and $Pr = 1$ for all kinds of problems.

We can construct the QGD numerical scheme for nonuniform space grids by replacing Δx , Δy , and Δz with $\Delta x_{i,j,k}$, $\Delta y_{i,j,k}$, and $\Delta z_{i,j,k}$. Here uniform space grids are presented for simplicity.

The presented numerical algorithm is simple because it is explicit, only central-difference approximations of the derivatives are used and additional monotoneization procedures as limiting functions are not required.

4. Solenoidal condition

In numerical solution of the QMHD system of equations it is necessary to satisfy the solenoidal condition for the magnetic field. A good approach for this is to use Faraday's law of induction:

$$\frac{\partial \mathbf{B}}{\partial t} = -\text{curl } \boldsymbol{\varepsilon}, \quad (32)$$

where $\boldsymbol{\varepsilon}$ is the electric field. On the right-hand side of (32) the magnetic diffusivity term (20) can be added. In our case we suppose $\nu_m = 0$.

This idea was used in a previously developed constrained transport method [36,38], whereby the components of the magnetic field, obtained from (4) (or (11) in the QMHD case), are replaced by the values from (32).

The electric field in the matter, moving with velocity \mathbf{u} , is

$$\boldsymbol{\varepsilon} = -[\mathbf{u}, \mathbf{B}], \quad (33)$$

and can be computed with the known values on the faces of cells (see Fig. 2), which should be shifted to the edges (see Fig. 3).

In the QMHD case, the constrained transport method is modified so that expression (33) transforms to another one, which contains τ -terms:

$$\boldsymbol{\varepsilon} = -[\mathbf{u}, \mathbf{B}] - [\mathbf{u}, \Delta \mathbf{B}] - [\Delta \mathbf{u}, \mathbf{B}]. \quad (34)$$

The components of $\boldsymbol{\varepsilon}$ from (34) can be rewritten according to (5) with QMHD corrections (12) as

$$\begin{aligned} \varepsilon_{xi,j+1/2,k} &= T_{yz}^m + T_{yz}^{mn}, \\ \varepsilon_{xi,j,k+1/2} &= -T_{zy}^m - T_{zy}^{mn}, \\ \varepsilon_{yi,j,k+1/2} &= T_{zx}^m + T_{zx}^{mn}, \\ \varepsilon_{yi+1/2,j,k} &= -T_{xz}^m - T_{xz}^{mn}, \\ \varepsilon_{zi+1/2,j,k} &= T_{xy}^m + T_{xy}^{mn}, \\ \varepsilon_{zi,j+1/2,k} &= -T_{yx}^m - T_{yx}^{mn}. \end{aligned} \quad (35)$$

A brief description of the constrained transport method is presented in the Appendix.

It is interesting to compare the QMHD algorithm presented with other known methods. This comparison is done below with a high-order PPML [5,6]. The comparison of the QMHD method with a robust Lax–Friedrichs method of the first order was done recently for a simplified case—a barotropic QGD system for 1D shallow water flows in the absence of magnetic fields [39]. This simplified case apparently allows one to study the advantages and disadvantages of both models. A Riemann problem for strong discontinuity with a height ratio of 50:1, a problem of shock formation in reflecting flow, and a problem of decay of a column of liquid were considered. The first two of these problems have exact solutions, which were used to determine accuracy and convergence of the algorithms. For all three tasks, it was shown that with a successful choice of α (in the first two cases $\alpha = 0.2$, in the last case $\alpha = 0.5$) the QGD algorithm significantly outperforms the accuracy of the Lax–Friedrichs scheme. At the same time, the QGD algorithm is roughly twice as effective in computation time than the implementation of the Lax–Friedrichs scheme used.

5. Discontinuous solutions

The numerical scheme described was verified on several distinctive MHD problems to check its convergence and accuracy for Euler equations. For all tests, a uniform grid with a constant step in each direction was set and the equation of state of an ideal gas was used. In the 1D case, all computations were performed on the interval $x \in [0, 1]$. Initial values of vector \mathbf{V} components, representing physical parameters, were defined on the left and right sides from the middle point of the interval as follows:

$$\mathbf{V} = \begin{cases} \mathbf{V}^L, & \text{if } x \leq 0.5, \\ \mathbf{V}^R, & \text{if } x > 0.5. \end{cases}$$

The number of numerical cells was equal to N , and the final time for computations was denoted as T . Boundary conditions were matched with corresponding initial conditions at the limits of the computational region. For every value of N , we calculate the relative error δ_N and the real order of accuracy R_N , using the following

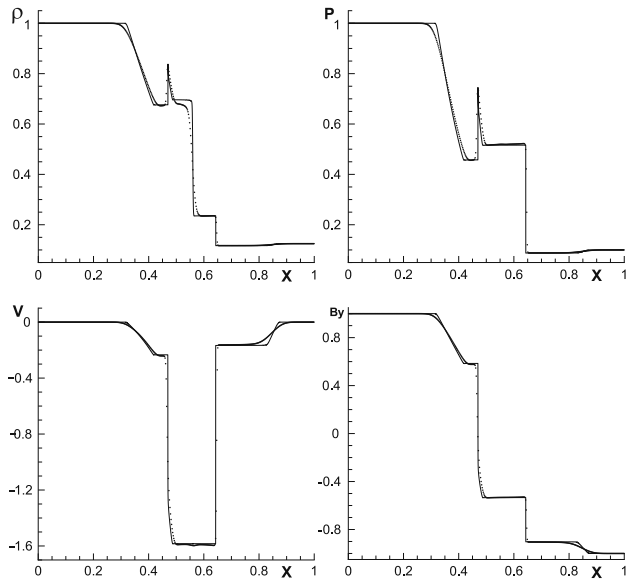


Fig. 4. Test 5.1. The result distributions of density, pressure, and y-components of the velocity and the magnetic field obtained on a grid with $N = 512$ in comparison with the exact solution (solid lines).

definitions:

$$\delta_N = \frac{1}{S} \sum_{k=1}^S E_N(V_k),$$

$$E_N(V_k) = \frac{\sum_{i=1}^N |V_{k,i} - V_{i,k}^{ex}|}{\sum_{i=1}^N |V_{k,i}^{ex}|},$$

$$R_N = \log_2(\delta_{N/2}/\delta_N), \tag{36}$$

where V^{ex} is an “exact” solution which is actually obtained on a very fine grid ($N = 20480$) by the same code, and S is the number of nonzero components of \mathbf{V} . In (36) the argument of logarithm is always positive. Negative values of R_N mean that the solution does not converge.

5.1. Riemann problem with initial discontinuity of the transverse component of the magnetic field

The initial conditions are given by [4]

$$(\rho^L, u_x^L, u_y^L, u_z^L, B_y^L, B_z^L, p^L) = (1.0, 0, 0, 0, 1.0, 0, 1.0),$$

$$(\rho^R, u_x^R, u_y^R, u_z^R, B_y^R, B_z^R, p^R) = (0.125, 0, 0, 0, -1.0, 0, 0.1).$$

The component of the magnetic field $B_x = 0.75$, the adiabatic index $\gamma = 2$, $N = 512$, and $T = 0.1$. The computational parameters are the Courant number $C = 0.2$ and regularization coefficient $\alpha = 0.4$. Computation results are presented in Fig. 4. In this problem, the solution of the QMHD system of equations consists of a fast rarefaction wave, moving to the left, an intermediate shock wave and a slow rarefaction wave, contact discontinuity, a slow shock wave, and one more fast rarefaction wave, moving to the right. Detailed discussion of this solution can be found in [3]. In the figures, the numerical solution is depicted by dots and the exact solution is shown as a solid line. The numerical scheme of the QMHD system accurately represents all physical discontinuities and the distribution behavior of all quantities without visible oscillations.

Notice that similar peaks in the density and pressure distributions, as we see in Fig. 4, are presented in many other computations

of this problem performed by high-order methods with limiters—see, for example, [5,40]. As can be seen from Table 1, with grid refinement the scheme error decreases at a rate typical of first-order schemes. We could decrease the relative errors by varying Sc and Pr .

The same test was performed in [5] with the PPML, which is formally third order accurate in space. The PPML results obtained on a grid with 512 cells are very similar to the results presented on Fig. 4, except for the region of contact discontinuity (see Fig. 3 in [5]). Numerical comparison does not show a significant superiority of the PPML: the average relative errors are 2–3 times smaller for the PPML, but the rate of convergence is similar (see Table 1). For this problem the PPML behaves like a first-order scheme. It resolves discontinuities better, but requires more computational cost than the QMHD method. Still, the QMHD method requires a more detailed computational grid to obtain a comparative quality of a solution.

For this test case the direct numerical estimation of condition (6) was performed. Time derivatives for every moment n and coordinate i were approximated as

$$\frac{\partial f}{\partial t} \Big|_i^n = \frac{f_i^{n+1} - f_i^{n-1}}{\Delta t_1 + \Delta t_2},$$

$$\frac{\partial}{\partial t} \tau \frac{\partial f}{\partial t} \Big|_i^n = \frac{1}{0.5(\Delta t_1 + \Delta t_2)} \left(\tau_i^{n+1/2} \frac{\partial f}{\partial t} \Big|_i^{n+1/2} - \tau_i^{n-1/2} \frac{\partial f}{\partial t} \Big|_i^{n-1/2} \right),$$

where

$$\frac{\partial f}{\partial t} \Big|_i^{n-1/2} = \frac{f_i^n - f_i^{n-1}}{\Delta t_1}, \quad \frac{\partial f}{\partial t} \Big|_i^{n+1/2} = \frac{f_i^{n+1} - f_i^n}{\Delta t_2},$$

$$\tau_i^{n\pm 1/2} = \frac{1}{2} (\tau_i^n + \tau_i^{n\pm 1}),$$

where Δt_1 and Δt_2 stand for time intervals between moments $n - 1 \rightarrow n$ and $n \rightarrow n + 1$, respectively.

As a result we obtained that the first-order time derivatives of all the variables considered dominate the second-order ones by a factor 50–1000 or more except for the neighborhood of the steepest contact discontinuity (Fig. 4, for $x \sim 0.65$), where the factor is about 5–20. Thus, the assumption used in the QMHD method that the second-order time derivatives are negligibly small is valid even at discontinuities.

5.2. Riemann problem with formation of all forms of discontinuities

Here the solution consists of two fast shock waves with speed equal to Mach numbers of 1.84 and 1.28 and directed to the left and to the right, respectively, two slow shock waves moving to the left and to the right with Mach numbers of 1.38 and 1.49, respectively, and one rotational and two contact discontinuities. The initial conditions are given by [4]

$$(\rho^L, u_x^L, u_y^L, u_z^L, B_y^L, B_z^L, p^L) = (0.18405, 3.8964, 0.5361,$$

$$2.4866, 2.394/\sqrt{4\pi}, 1.197/\sqrt{4\pi}, 0.3641),$$

$$(\rho^R, u_x^R, u_y^R, u_z^R, B_y^R, B_z^R, p^R)$$

$$= (0.1, -5.5, 0, 0, 2/\sqrt{4\pi}, 1/\sqrt{4\pi}, 0.1).$$

The component of the magnetic field $B_x = 4/\sqrt{4\pi}$, the adiabatic index $\gamma = 5/3$, $N = 512$, $T = 0.15$, the Courant number $C = 0.2$, and the regularization coefficient $\alpha = 0.5$. Computation results are presented in Fig. 5.

Table 1

Test 5.1. The average relative errors and the rates of convergence at $T = 0.1$ for the QMHD method and the PPML.

N	$Sc = 1, Pr = 1$		$Sc = 0.5, Pr = 1$		$Sc = 1, Pr = 0.5$		PPML	
	$\delta_N, 10^{-2}$	R_N						
128	7.416	–	6.496	–	7.495	–	3.346	–
256	4.844	0.614	4.167	0.641	4.904	0.612	1.929	0.795
512	2.851	0.765	2.344	0.830	2.906	0.755	0.8839	1.126
1024	1.761	0.695	1.436	0.710	1.798	0.963	0.4863	0.862

Table 2

Test 5.2. The average relative errors and the rates of convergence at $T = 0.15$ for the QMHD method and the PPML.

N	$Sc = 1, Pr = 1$		$Sc = 0.5, Pr = 1$		$Sc = 1, Pr = 0.5$		PPML	
	$\delta_N, 10^{-2}$	R_N						
128	6.951	–	5.625	–	7.079	–	6.244	–
256	4.353	0.675	3.415	0.720	4.469	0.664	4.047	0.626
512	2.612	0.737	2.013	0.763	2.689	0.733	2.540	0.672
1024	1.585	0.721	1.213	0.731	1.632	0.720	1.637	0.634

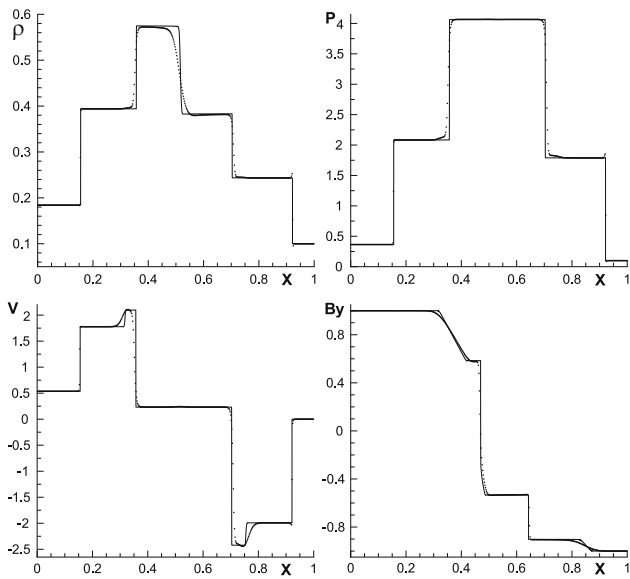


Fig. 5. Test 5.2. The distributions of density, pressure, and y-components of the velocity and the magnetic field obtained on a grid with $N = 512$ in comparison with the exact solution (solid lines).

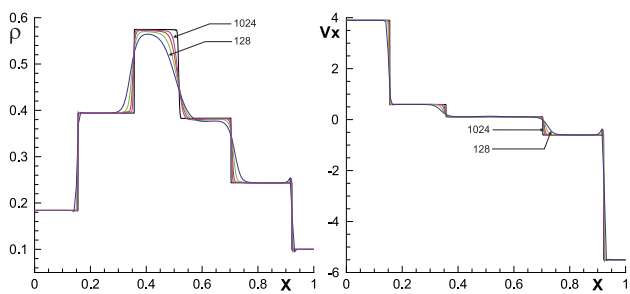


Fig. 6. Test 5.2. Grid convergence for the example of the density and x-component of the velocity. The computations were performed on grids with $N = 128$ up to $N = 1024$ cells.

Convergence of the numerical solution to exact one by consecutive reduction of the grid step by 2 times for the density and the velocity profiles is shown in Fig. 6. An accurate distribution of the density is achieved on fine grids, whereas the velocity and pressure profiles are well resolved even on rougher grids. Table 2 gives the average relative errors and the rate of convergence for this test obtained in calculations with varying Sc and Pr . The results for the PPML are presented for comparison. Here the PPML shows similar

values of average relative errors and an even worse result for the rate of convergence.

6. Smooth solutions

6.1. Propagation of MHD waves in the 2D case

The following tests aim to investigate smooth solutions (fast, slow, and Alfvén waves). In these tests, the actual order of the difference scheme must be in correspondence with the order of the approximation. Here, unlike the previous tests for discontinuous solutions, by definition a high-order scheme must demonstrate higher accuracy than the first-order scheme.

The following problem is a perfect quantitative test to determine accuracy and convergence order of a numerical algorithm.

All physical parameters in the entire computational domain are equal to constant values and are chosen so that main waves are sufficiently distinct and the wave vector is directed at some angle to the magnetic field. The waves are specified as perturbations to initial constant values of physical quantities in the following form:

$$\delta \mathbf{U} = A \mathbf{R} \sin(2\pi x).$$

Here, $\mathbf{U} = [\rho, \mathbf{u}_x, \mathbf{u}_y, \mathbf{u}_z, \mathbf{E}, \mathbf{B}_y, \mathbf{B}_z]$ is the vector of conservative variables, A is a magnitude, \mathbf{R} is the given right eigenvector in conserved variables for a wave mode under consideration in hyperbolic MHD system matrix. In all cases, $A = 10^{-6}$. The size of the computational domain is equal to one wavelength. Periodic boundary conditions are used for all variables. The error of the numerical solution is measured by norm estimation after the wave passes a distance equal to one wavelength. In this case the initial state is evolved for a time $T = \lambda/c$, where λ is the wavelength, and c is the speed of the wave mode under consideration. For each component of the conserved variable, we calculate the error with respect to the initial conditions. The expressions for error estimation are

$$\|\delta \mathbf{U}\| = \sqrt{\sum_{k=1}^S (\delta U_k)^2}, \quad \delta U_k = \frac{1}{N^2} \sum_{j=1}^N \sum_{i=1}^N |U_{k,i,j}^n - U_{k,i,j}^0|.$$

Here $U_{k,i,j}^n$ is a numerical solution for the k th component of the vector of conservative variables for each point (i, j) at the time moment n , $U_{k,i,j}^0$ is an initial value, S is the number of vector components, and N represents the number of points in the domain, which is set equal in each direction. The initial conditions are given by [36,41]

$$\rho = 1, \quad p = \frac{1}{\gamma}, \quad b_x = 1, \quad b_y = \sqrt{2}, \quad b_z = 0.5,$$

where $b = B/\sqrt{4\pi}$ and $\gamma = 5/3$.

Table 3

Test 6.1. The average relative errors and the rates of convergence after the wave passes a distance equal to one wavelength.

N	Fast magnetosonic wave		Alfvén wave		Slow magnetosonic wave	
	$\ \delta\mathbf{U}\ , 10^{-8}$	R_N	$\ \delta\mathbf{U}\ , 10^{-8}$	R_N	$\ \delta\mathbf{U}\ , 10^{-8}$	R_N
64	15.395	–	5.6148	–	12.508	–
128	8.1368	0.9199	2.9196	0.9435	6.6601	0.9092
256	4.1871	0.9585	1.4920	0.9685	3.4399	0.9532
512	2.1243	0.9790	0.75461	0.9834	1.7485	0.9762
1024	1.0700	0.9894	0.37953	0.9915	0.88157	0.9880
2048	0.53696	0.9947	0.19033	0.9957	0.44262	0.9940

The values of the components of the right eigenvectors are equal to

$$\mathbf{R} = (0.4472135954999580, -0.8944271909999160, 0.4216370213557840, 0.1490711984999860, 2.012457825664615, 0.8432740427115680, 0.2981423969999720)$$

for a fast magnetosonic wave moving to the left,

$$\mathbf{R} = (0, 0, -0.3333333333333333, 0.9428090415820634, 0, -0.3333333333333333, 0.9428090415820634),$$

for an Alfvén wave moving to the left, and

$$\mathbf{R} = (0.8944271909999159, -0.4472135954999579, -0.8432740427115680, -0.2981423969999720, 0.6708136850795449, -0.4216370213557841, -0.1490711984999860)$$

for a slow magnetosonic wave moving to the left, where the components of the right eigenvectors correspond to the ordering of the conservative parameters' vector \mathbf{U} .

The fast, Alfvén, and slow wave speeds are equal to 2, 1, and 0.5, respectively. The absolute error in propagation of each of these waves and the order of numerical algorithm accuracy are presented in Table 3. Our algorithm has an actual order of accuracy close to 1 on smooth solutions for all problems considered.

6.2. Numerical dissipation and decay of Alfvén waves

In numerical modeling with a space grid, any numerical scheme always has some dissipation. To estimate the level of numerical dissipation of the QMHD scheme, a test on decay of Alfvén waves was performed [42]. At the initial moment of time, the Alfvén wave has the following parameters

$$\delta u_x = u_{\text{amp}} c_a \sin(k_x x + k_y y),$$

and moves on a fixed background with $\rho_0 = 1, p_0 = 1, B_x = 1,$ and $B_y = B_z = 0$.

The computational domain represents a square of side $L = 1$. The initial Alfvén wave speed is $c_a = 0.7071$ and its magnitude is $u_{\text{amp}} = 0.1$, the adiabatic index is $\gamma = 5/3$, and periodic boundary conditions were applied. The basic computation was done with the Courant number $C = 0.3, \alpha = 0.1$, and a grid of $N = 128$ in each direction. Fig. 7 shows the time evolution of the maximum of the magnetic field z-component in computations on a sequence of twice-refined grids ($N = 64, 128, 256$) until time $T = 10$. For the grid with $N = 128$ and $Sc = 1, \alpha$ changed from 0.5 to 0.1; for the grid with $N = 128$ and $\alpha = 0.1, Sc$ changed from 1 to 0.4. The best case, $\alpha = 0.1$ and $Sc = 0.4$, was once again recomputed on a twice more refined grid with $N = 256$.

The dissipation level corresponds to the schemes of first order in space and time, and quickly decreases with grid refinement. For the given Courant number and number of grid cells, dissipation of the numerical scheme decreases as the α and Sc decrease.

The smallest dissipation level of the numerical scheme, wherein solution stability is preserved, corresponds to $\alpha = 0.1$ and $Sc = 0.4$ on a grid with $N = 128$. In this case, the computational results are similar to the results obtained by the PPML for $N = 64$ (see Fig. 11 in [6]). For the same quality, we need only a 2 times finer grid, not a 3–4 times finer grid.

6.3. Propagation of a circularly polarized Alfvén wave

This test problem was considered in [43] to study the accuracy and the order of convergence of numerical schemes on smooth solutions. The Alfvén wave propagates along the diagonal of the grid at an angle $\theta = \tan^{-1}(0.5) \approx 26.6^\circ$ to the x-axis. The computational domain has a size of $0 < x < 1/\cos\theta, 0 < y < 1/\sin\theta$, with $N \times N$ cells. Since the wave does not move along diagonals of discrete cells, the problem has a real multidimensional nature. The initial conditions are given by

$$\begin{aligned} \rho &= 1, & u_{\parallel} &= 0, & u_{\perp} &= 0.1 \sin(2\pi\xi), \\ u_z &= 0.1 \cos(2\pi\xi), \\ p &= 0.1, & B_{\parallel} &= 1, & B_{\perp} &= 0.1 \sin(2\pi\xi), \\ B_z &= 0.1 \cos(2\pi\xi), \end{aligned}$$

where $\xi = x \cos\theta + y \sin\theta$. Here, u_{\parallel}, u_{\perp} and B_{\parallel}, B_{\perp} are components of the velocity and the magnetic field directed parallel and perpendicular to the direction of the Alfvén wave movement. For example,

$$B_{\parallel} = B_x \cos\theta + B_y \sin\theta, \quad B_{\perp} = B_y \cos\theta - B_x \sin\theta.$$

The wave propagates toward a point $(x, y) = (0, 0)$ with speed $B_{\parallel}/\sqrt{\rho} = 1$. Also, computations were performed for the case of the stationary Alfvén wave with $u_{\parallel} = 1$ in the initial conditions. The problem was solved with $N = 16, 32, 64, 128,$ and 256 in both directions, and the relative numerical error was estimated for each quantity by the formula

$$\delta_N(U) = \frac{\sum_{i=1}^N \sum_{j=1}^N |U_{i,j}^N - U_{i,j}^{\text{ex}}|}{\sum_{i=1}^N \sum_{j=1}^N |U_{i,j}^{\text{ex}}|}, \quad U = u_{\perp}, u_z, B_{\perp}, B_z,$$

where $U_{i,j}^{\text{ex}}$ is the exact solution. The convergence order of the scheme was estimated according to (36), where δ_N was defined as the mean by

$$\delta_N = \frac{1}{4} (\delta_N(u_{\perp}) + \delta_N(u_z) + \delta_N(B_{\perp}) + \delta_N(B_z)).$$

The computations were done until time $T = 5$ with the Courant number $C = 0.3, \alpha = 0.1$, the adiabatic index $\gamma = 5/3$, and periodic boundary conditions.

In Fig. 8 the orthogonal component B_{\perp} of the magnetic field is presented in computations on various grids for propagating and stationary Alfvén waves. The values of N are indicated by numbers. It can be seen that the numerical solution of the problem tends to the exact solution with increasing N . In Table 4, the average relative

Table 4
Test 6.3. The average relative errors and the rates of convergence.

N	Propagating ($u_{ } = 0$)		Stationary ($u_{ } = 1$)		$u_{ } = 1$ Flux-CT/CD [43]	
	δ_N	R_N	δ_N	R_N	δ_N	R_N
	8	1.697	–	0.1234	–	0.315
16	0.9070	0.9038	7.539×10^{-2}	0.7109	0.122	1.368
32	0.3435	1.401	3.914×10^{-2}	0.9457	3.7×10^{-2}	1.721
64	0.1489	1.206	1.975×10^{-2}	0.9868	1.3×10^{-2}	1.509
128	7.203×10^{-2}	1.048	9.916×10^{-3}	0.9940	–	–
256	3.605×10^{-2}	0.9986	4.968×10^{-3}	0.9971	–	–

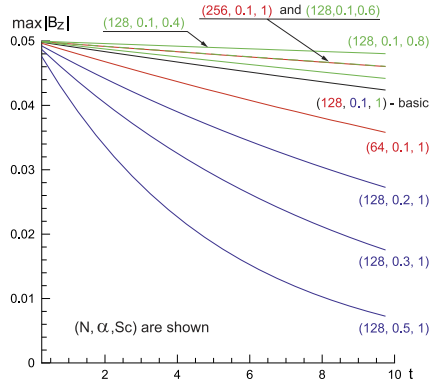


Fig. 7. Test 6.2: Time evolution of the maximum of the magnetic field z-component in computations on various grids, for different α and Schmidt numbers.

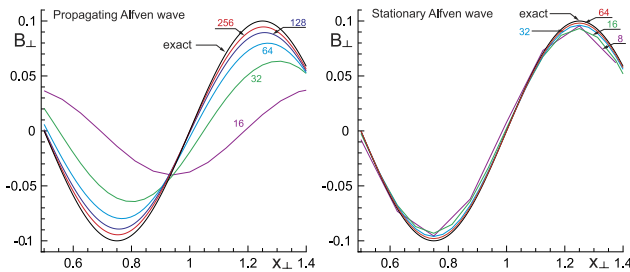


Fig. 8. Test 6.3: Orthogonal component of the magnetic field in the computations on various grids for a propagating Alfvén wave (left) and for a stationary Alfvén wave (right). The values of N are indicated by numbers.

error and the order of convergence are shown. These are compared with the second-order in space constrained transport/central difference (CT/CD) scheme from [43] which apparently showed higher accuracy (the actual order of CT/CD is 1.4–1.7). The results obtained confirm that with increasing of the resolution, the QMHD scheme tends to first order of accuracy in space and time. Still, by comparing the QMHD average relative errors with the errors of the CT/CD scheme, we note that the QMHD scheme gives similar errors for grids of $N = 32$ and 64 , and even better results for $N = 8$ and 16 (Table 4).

7. Complex flows

7.1. Orszag–Tang vortex

In this problem, the formation of the complex structure of shock waves in supersonic turbulence is considered [44,45]. This is a hard problem for many numerical schemes since the appearing gradients of the quantities, which are especially strong in the central part of the computational domain, could lead to oscillations and negative density values.

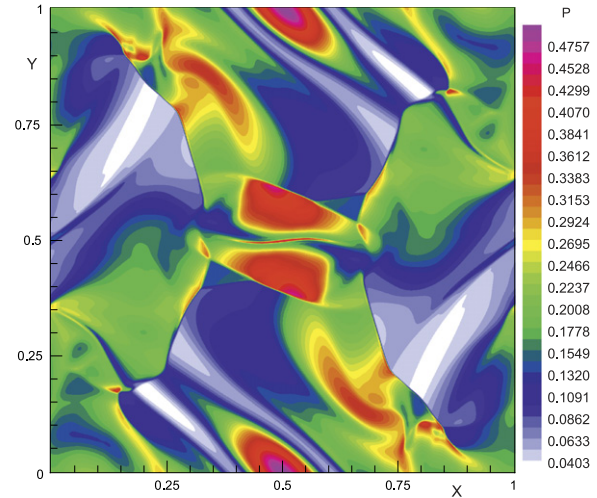


Fig. 9. Test 7.1. Distributions of pressure on a 512×512 grid at $T = 0.5$.

The problem is solved in the square domain with side $L = 1$. The initial conditions are given by

$$\begin{aligned} \rho &= 25/(36\pi), p = 5/(12\pi), \\ u_x &= -\sin(2\pi y), u_y = \sin(2\pi x), u_z = 0, \\ B_x &= -B_0 \sin(2\pi y), B_y = B_0 \sin(4\pi x), B_z = 0, \end{aligned}$$

where $B_0 = 1/\sqrt{4\pi}$. A solution is computed up to time $T = 0.5$ on a 512×512 grid with Courant number $C = 0.4$, $\alpha = 0.2$, and adiabatic index $\gamma = 5/3$. Periodic boundary conditions are applied.

The resulting distributions of pressure and magnetic energy are shown in Figs. 9 and 10. The structure of the flow obtained preserves all the shocks with high accuracy. The levels of constant values show that the symmetry of the flow is perfectly conserved, which is very important for investigation of turbulence. Some inviscid invariants such as helicity (in three dimensions) and enstrophy (in two dimensions) are fundamentally related to the symmetry of the turbulent flow. Helicity expresses the correlation between the velocity and its curl, and is conserved as well as a numerical scheme conserves mirror symmetry [46]. Also the better symmetry properties of differential operators are reproduced by the difference approximation, the greater the accuracy of the smallest scales of motion that could be achieved, since the behavior of turbulent flow on small scales is a result of a delicate balance between convective transport and diffusive dissipation [47].

Figs. 11 and 12 show distributions of pressure along the lines $y = 0.3125$ and $y = 0.4277$ obtained on a sequence of twice-refined grids. The solution on the grid with $N = 1024$ is depicted by the black line. Starting from $N = 128$, the QMHD scheme gives a solution of sufficient quality, representing all the existent shocks. It is also confirmed by Table 5, where the average relative errors and the rates of convergence are shown in relation to the solution with $N = 1024$, regarded as an “exact” solution. These were computed

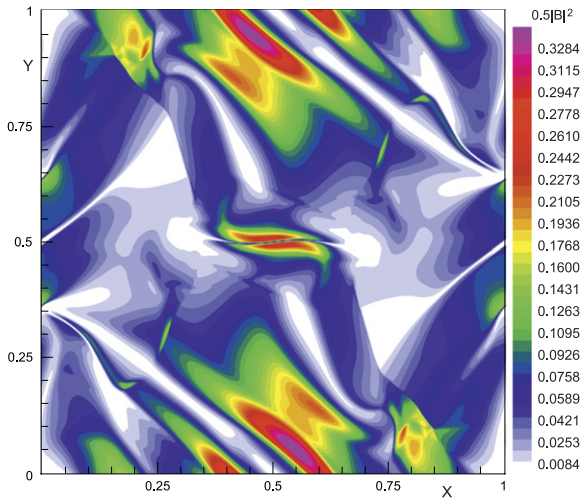


Fig. 10. Test 7.1. Distributions of magnetic energy on a 512×512 grid at $T = 0.5$.

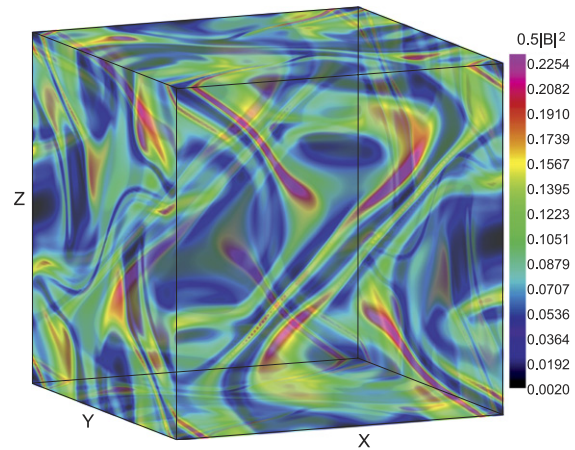


Fig. 13. Test 7.1. Three-dimensional Orszag–Tang vortex problem. Distribution of magnetic field energy in a 3D plot for $T = 0.5$.

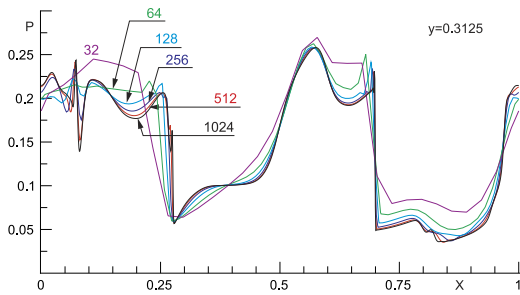


Fig. 11. Test 7.1. Pressure along the line $y = 0.3125$ on various grids at $T = 0.5$.

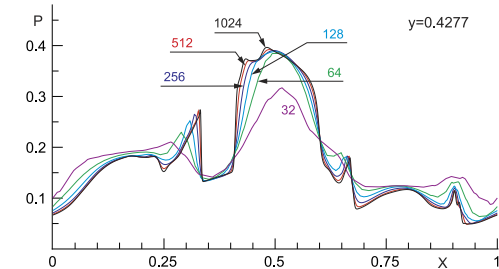


Fig. 12. Test 7.1. Pressure along the line $y = 0.4277$ on various grids at $T = 0.5$.

Table 5
Test 7.1. The average relative errors and the rates of convergence at $T = 0.5$.

N	δ_N	R_N
32	0.2433	–
64	0.1634	0.574
128	9.779×10^{-2}	0.741
256	5.289×10^{-2}	0.887
512	2.145×10^{-2}	1.30

for all nonzero quantities in the whole 2D domain. In this difficult test case the actual order of the scheme increases with the number of dots and reaches a value of 1.30 (Table 5).

Compared with the results obtained with the high-order PPML [6], we can say that for this problem the rate of convergence of the QMHD scheme is similar to that of the PPML. Still, the PPML gives smaller average relative errors: $\delta_N = 4.5204 \times 10^{-2}$ for $N = 100$ and $\delta_N = 1.9262 \times 10^{-2}$ for $N = 200$ (see Table 2 in [6]).

For the first time we suggest extending the Orszag–Tang vortex problem to the 3D case with all nonzero initial components of

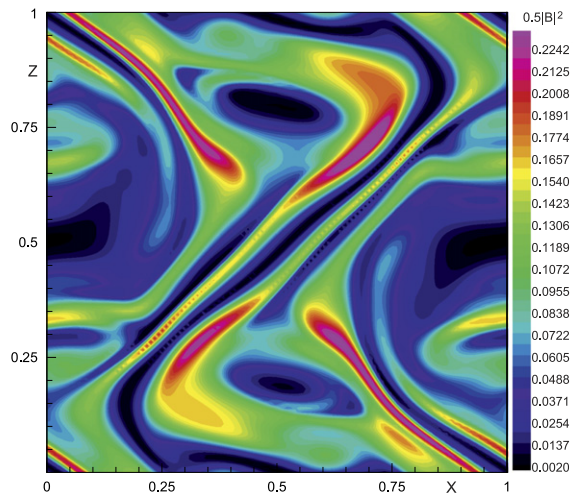


Fig. 14. Test 7.1. Three-dimensional Orszag–Tang vortex problem. Distribution of magnetic field energy on a 2D slice along the plane $y = 0$.

the velocity and magnetic field, defined as functions of transverse space coordinates with the following initial conditions:

$$\rho = 25/(36\pi), p = 5/(12\pi),$$

$$u_x = -\sin(2\pi z), u_y = \sin(2\pi x), u_z = \sin(2\pi y),$$

$$B_x = -B_0 \sin(2\pi z), B_y = B_0 \sin(4\pi x), B_z = B_0 \sin(4\pi y).$$

The simulation is performed in a cubic domain on a grid of $N^3 = 120^3$. The parameters for the 3D case are chosen as $\alpha = 0.5$ and $C = 0.1$.

The solution for $T = 0.5$ is presented in Figs. 13 and 14, where the magnetic field energy is shown. The QMHD scheme allows one to obtain the correct structure with all the discontinuities and to perform the simulation for infinitely long time. In the long-time simulation the flow decays into small structures and the kinetic energy dissipates with time because of viscosity.

7.2. Propagation of a blast wave through a magnetized medium

In this problem, propagation of the initial finite perturbation of the pressure through a medium with a superimposed magnetic field [48] is investigated. The problem is solved in the cubic computational domain with side dimension $L = 1$ and $N^3 = 120^3$ cells. In the initial moment, density $\rho = 1$ and pressure $p = 1$ in the entire domain, except for the central part with radius $r = 0.05$, where the pressure is $p = 1000$. A uniform magnetic field with

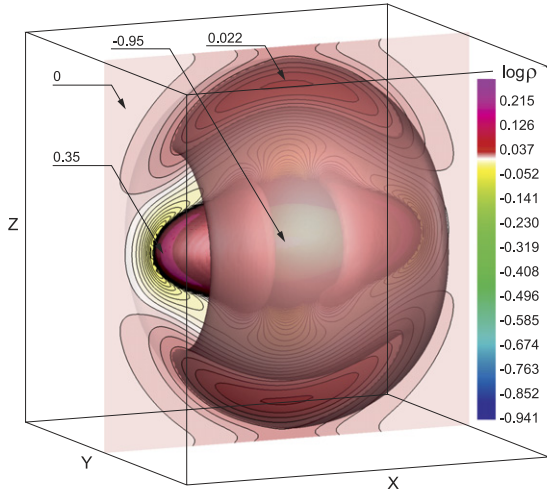


Fig. 15. Test 7.2. A blast wave in a magnetized medium in three dimensions. Distribution of the logarithm of the density in a 3D plot for $T = 0.03$. The values in the representative regions are shown by figures.

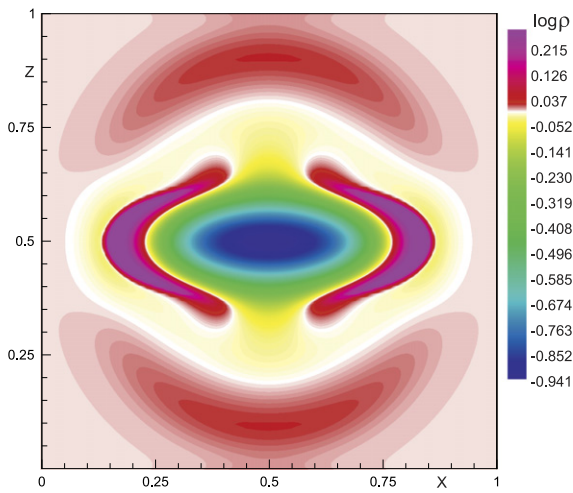


Fig. 16. Test 7.2. A blast wave in a magnetized medium in three dimensions. Distribution of the logarithm of the density on a 2D slice along the plane $y = 0$.

magnitude $B = 10$ is directed along the x -axis. The adiabatic index $\gamma = 1.4$. Computations were done until $T = 0.03$ with Courant number $C = 0.1$ and $\alpha = 0.5$. The gradients of all parameters were zero at the domain boundary.

Figs. 15 and 16 present the resulting numerical solution. A magnetic field introduces anisotropy in expansion of a substance. Under the action of the pressure, the expansion accelerates along magnetic field lines, and shock waves with higher kinetic and magnetic energy can be seen at the boundary in the middle part of the domain. A rarefied area with lower density and pressure and the prevalence of magnetic energy over the kinetic and thermal energy forms at the center of the computational domain. In spite of the large initial difference in the pressure and high magnetization of the medium in the middle part of the computational domain, the QMHD scheme provides positive values of the pressure and density, and describes all intrinsic discontinuities with good accuracy for the scheme of first order in space and time at the final stage of substance expansion.

8. Conclusions

We have presented an extension of the QGD approach for the solution of problems of ideal magnetohydrodynamics. We

obtained the regularized, or QGD (QMHD), system of equations for ideal magnetohydrodynamics by applying temporal averaging to all physical parameters, including the magnetic field. The numerical QMHD scheme is multidimensional, where evolution of all physical quantities is done in a unsplit form by space directions.

We showed that on the basis of a unified approach, the QMHD computational method applied for compressible magnetohydrodynamics allows the modeling of a wide range of nonstationary MHD problems. For all test cases studied, computations show steady convergence of the numerical solution to its exact solution with shredding of the space grid, providing an accurate representation of the distribution for all physical quantities on the smooth part of a solution and on discontinuities as well. By adjustment of the tuning parameters, the quality of the numerical solution may be increased.

The tests of the Orszag–Tang vortex and blast wave propagation through a magnetized medium were solved in the full 3D case. The values of the tuning parameters $\alpha = 0.5$ and $Sc = Pr = 1$ are suitable for all problems in 1D, 2D, and 3D cases.

The disadvantage of the QMHD method is the first-order approximation that requires a more detailed computational grid to obtain a solution of quality similar to that produced by a high-order scheme. The average relative errors produced by the shock-captured high-order PPML scheme and by the first-order QMHD scheme usually differ by about 2–3 times depending on the problem (or could be even similar for some cases). On the other hand, the high approximation orders are a little bit formal since they are true only for smooth solutions, whereas in most interesting applications the solutions are discontinuous. This was demonstrated by test problems 5.1 and 5.2 with strong discontinuities, where the PPML behaved like a first-order scheme.

The QMHD method is robust, relatively cheap in computational cost, and requires no Riemann solvers and no additional monotization procedures—for example, limiting functions, which is a very nice property especially for MHD simulations. The simplicity of numerical realization and the uniformity of the algorithm provide a natural realization on parallel computer systems using domain-decomposition technique. This allows one to use the QMHD approach for “big” problems, where very large computational grids are required. The robustness, simplicity, and computational effectiveness of the QMHD approach make it very promising for use in simulations of complex 3D flows with strong magnetic fields in a wide range of “difficult” engineering and scientific problems.

Acknowledgments

This project has received funding from the European Union’s Seventh Framework Programme for research, technological development, and demonstration under grant agreement no. 320478. The work was supported by the Russian Foundation for Basic Research (project no. 13-01-00703-a).

Appendix

According to the constrained transport method, the components (35) are transported to the edge centers of the cells (see Fig. 3) as

$$\begin{aligned} \mathcal{E}_{z\ i+1/2,j+1/2,k} = & \frac{1}{4} (\mathcal{E}_{z\ i+1/2,j,k} + \mathcal{E}_{z\ i+1/2,j+1,k} \\ & + \mathcal{E}_{z\ i,j+1/2,k} + \mathcal{E}_{z\ i+1,j+1/2,k}) \\ & + \frac{\Delta y}{8} \left(\left. \frac{\partial \mathcal{E}_z}{\partial y} \right|_{i+1/2,j+1/4,k} - \left. \frac{\partial \mathcal{E}_z}{\partial y} \right|_{i+1/2,j+3/4,k} \right) \\ & + \frac{\Delta x}{8} \left(\left. \frac{\partial \mathcal{E}_z}{\partial x} \right|_{i+1/4,j+1/2,k} - \left. \frac{\partial \mathcal{E}_z}{\partial x} \right|_{i+3/4,j+1/2,k} \right), \end{aligned} \quad (37)$$

where the corresponding derivatives are computed depending on the sign of the velocity on the face:

$$\frac{\partial \mathcal{E}_z}{\partial y} \Big|_{i+1/2, j+1/4, k} = \begin{cases} \frac{\partial \mathcal{E}_z}{\partial y} \Big|_{i, j+1/4, k}, & u_{xi+1/2, j, k} > 0, \\ \frac{\partial \mathcal{E}_z}{\partial y} \Big|_{i+1, j+1/4, k}, & u_{xi+1/2, j, k} < 0, \\ \frac{1}{2} \left(\frac{\partial \mathcal{E}_z}{\partial y} \Big|_{i, j+1/4, k} + \frac{\partial \mathcal{E}_z}{\partial y} \Big|_{i+1, j+1/4, k} \right), & \text{otherwise,} \end{cases}$$

with the differential expressions in the form

$$\frac{\partial \mathcal{E}_z}{\partial y} \Big|_{i, j+1/4, k} = 2 \left(\frac{\mathcal{E}_{zi, j+1/2, k} - \mathcal{E}_{zi, j, k}}{\Delta y} \right).$$

The values of the components of the electric field at the edge centers of the cells that are obtained are used in (32) to compute the magnetic field components at the face centers at the next time point $t + \Delta t$ (Fig. 17). The corresponding differential approximation has the form

$$\begin{aligned} \hat{B}_{xi+1/2, j, k} &= B_{xi+1/2, j, k} \\ &\quad - \frac{\Delta t}{\Delta y} (\mathcal{E}_{zi+1/2, j+1/2, k} - \mathcal{E}_{zi+1/2, j-1/2, k}) \\ &\quad + \frac{\Delta t}{\Delta z} (\mathcal{E}_{yi+1/2, j, k+1/2} - \mathcal{E}_{yi+1/2, j, k-1/2}), \end{aligned}$$

$$\begin{aligned} \hat{B}_{yi, j+1/2, k} &= B_{yi, j+1/2, k} \\ &\quad + \frac{\Delta t}{\Delta x} (\mathcal{E}_{zi+1/2, j+1/2, k} - \mathcal{E}_{zi-1/2, j+1/2, k}) \\ &\quad - \frac{\Delta t}{\Delta z} (\mathcal{E}_{xi, j+1/2, k+1/2} - \mathcal{E}_{xi, j+1/2, k-1/2}), \end{aligned}$$

$$\begin{aligned} \hat{B}_{zi, j, k+1/2} &= B_{zi, j, k+1/2} \\ &\quad - \frac{\Delta t}{\Delta x} (\mathcal{E}_{yi+1/2, j, k+1/2} - \mathcal{E}_{yi-1/2, j, k+1/2}) \\ &\quad + \frac{\Delta t}{\Delta y} (\mathcal{E}_{xi, j+1/2, k+1/2} - \mathcal{E}_{xi, j-1/2, k+1/2}). \end{aligned}$$

The values of the components of the magnetic field at the centers of the cells are obtained from simple averaging (Fig. 18):

$$\begin{aligned} \hat{B}_{xi, j, k} &= \frac{1}{2} (\hat{B}_{xi+1/2, j, k} + \hat{B}_{xi-1/2, j, k}), \\ \hat{B}_{yi, j, k} &= \frac{1}{2} (\hat{B}_{yi, j+1/2, k} + \hat{B}_{yi, j-1/2, k}), \\ \hat{B}_{zi, j, k} &= \frac{1}{2} (\hat{B}_{zi, j, k+1/2} + \hat{B}_{zi, j, k-1/2}). \end{aligned} \quad (38)$$

The magnetic field obtained according to (38) is divergence free. This can be shown by computation of the divergence in the apices of the cells as

$$\begin{aligned} \text{div } \hat{\mathbf{B}} \Big|_{i+1/2, j+1/2, k+1/2} &= \frac{1}{4\Delta x} (\hat{B}_{xi+1, j, k} + \hat{B}_{xi+1, j+1, k} - \hat{B}_{xi, j, k} - \hat{B}_{xi, j+1, k}) \\ &\quad + \frac{1}{4\Delta y} (\hat{B}_{xi+1, j, k+1} + \hat{B}_{xi+1, j+1, k+1} - \hat{B}_{xi, j, k+1} - \hat{B}_{xi, j+1, k+1}) \\ &\quad + \frac{1}{4\Delta y} (\hat{B}_{yi, j+1, k} + \hat{B}_{yi, j+1, k+1} - \hat{B}_{yi, j, k} - \hat{B}_{yi, j+1, k}) \\ &\quad + \frac{1}{4\Delta y} (\hat{B}_{yi, j+1, k+1} + \hat{B}_{yi, j+1, k+1} - \hat{B}_{yi, j, k+1} - \hat{B}_{yi, j+1, k+1}) \\ &\quad + \frac{1}{4\Delta z} (\hat{B}_{zi, j, k+1} + \hat{B}_{zi, j+1, k+1} - \hat{B}_{zi, j, k} - \hat{B}_{zi, j+1, k}) \\ &\quad + \frac{1}{4\Delta z} (\hat{B}_{zi, j+1, k+1} + \hat{B}_{zi, j+1, k+1} - \hat{B}_{zi, j+1, k} - \hat{B}_{zi, j+1, k+1}). \end{aligned}$$

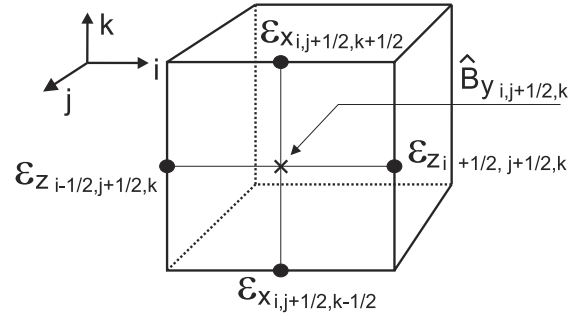


Fig. 17. Computation of the magnetic field components at the time point $t + \Delta t$ at the face centers of the cells according to Faraday's law of induction.

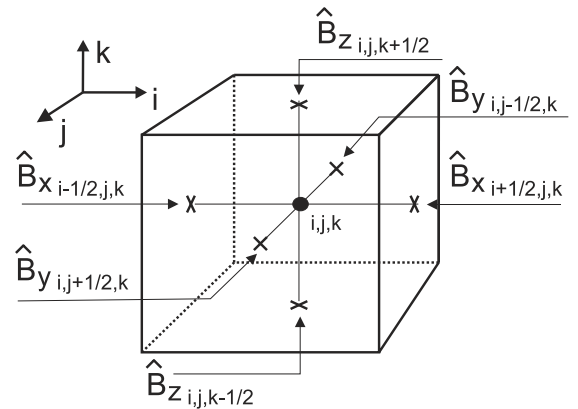


Fig. 18. Computation of the components of magnetic field at the time point $t + \Delta t$ at the cell centers.

Note that the algorithm described gives a shifted distribution of the magnetic field relative to the distribution of hydrodynamic quantities. This could be important for some tests on rough grids—for example, in the case of propagation of a circularly polarized Alfvén wave in 2D space, where the comparison between the components of the magnetic field obtained on a rough grid and a known analytical solution should be done. To study such problems, the algorithm could be modified in the following way. The electric field components, computed at the edge centers of the cells as in (37), should be shifted to the face centers by averaging. In the 2D case this gives

$$\mathcal{E}_{zi+1/2, j} = \frac{1}{2} (\mathcal{E}_{zi+1/2, j+1/2} + \mathcal{E}_{zi+1/2, j-1/2}),$$

$$\mathcal{E}_{zi, j+1/2} = \frac{1}{2} (\mathcal{E}_{zi+1/2, j+1/2} + \mathcal{E}_{zi-1/2, j+1/2}).$$

Then, Faraday's law of induction should be applied:

$$\hat{B}_{xi, j} = B_{xi, j} - \frac{\Delta t}{\Delta y} (\mathcal{E}_{zi, j+1/2} - \mathcal{E}_{zi, j-1/2}),$$

$$\hat{B}_{yi, j} = B_{yi, j} + \frac{\Delta t}{\Delta x} (\mathcal{E}_{zi+1/2, j} - \mathcal{E}_{zi-1/2, j}).$$

References

- [1] H. Yu, Y.-P. Liu, A second-order accurate, component-wise TVD scheme for nonlinear, hyperbolic conservation laws, *J. Comput. Phys.* 173 (2001) 1–16.
- [2] G. Tóth, D. Odstrčil, Comparison of some flux corrected transport and total variation diminishing numerical schemes for hydrodynamic and magnetohydrodynamic problems, *J. Comput. Phys.* 128 (1996) 82–100.
- [3] G.S. Jiang, C.C. Wu, A high-order WENO finite difference scheme for the equations of ideal magnetohydrodynamics, *J. Comput. Phys.* 150 (1999) 561–594.
- [4] W. Dai, P. Woodward, Extension of the piecewise parabolic method to multidimensional ideal magnetohydrodynamics, *J. Comput. Phys.* 115 (1994) 485–514.

- [5] M.V. Popov, S.D. Ustyugov, Piecewise parabolic method on local stencil for ideal magnetohydrodynamics, *Comput. Math. Math. Phys.* 48 (2008) 477–499.
- [6] S.D. Ustyugov, M.V. Popov, A.G. Kritsuk, M.L. Norman, Piecewise parabolic method on a local stencil for magnetized supersonic turbulence simulation, *J. Comput. Phys.* 228 (2009) 7614–7633.
- [7] M. Brio, C.C. Wu, An upwind differencing scheme for the equations of ideal magnetohydrodynamics, *J. Comput. Phys.* 75 (1988) 400–422.
- [8] S. Li, An HLLC Riemann solver for magnetohydrodynamics, *J. Comput. Phys.* 203 (2005) 344–357.
- [9] T. Miyoshi, K. Kusano, A multi-state HLL approximate Riemann solver for ideal magnetohydrodynamics, *J. Comput. Phys.* 208 (2005) 315–344.
- [10] B. Fryxell, et al., FLASH: an adaptive mesh hydrodynamics code for modeling astrophysical thermonuclear flashes, *Astrophys. J. Suppl. Ser.* 131 (2000) 273–334.
- [11] B. O’Shea, et al., Introducing Enzo, an AMR cosmology application // adaptive mesh refinement – theory and applications, in: *Lect. Notes Comput. Sci. Eng.*, vol. 41, Springer-Verlag, Berlin, 2005, pp. 341–350. [astro-ph/0403044].
- [12] J.M. Stone, T.A. Gardiner, P. Teuben, et al., Athena: a new code for astrophysical MHD, *Astrophys. J. Suppl. Ser.* 178 (2008) 137–177.
- [13] A.S. Almgren, et al., CASTRO: a new compressible astrophysical solver. I. Hydrodynamics and self-gravity, *Astrophys. J.* 715 (2010) 1221–1238.
- [14] B.N. Chetverushkin, Kinetic Schemes and Quasi-Gas Dynamic System of Equations, CIMNE, Barcelona, 2008.
- [15] T.G. Elizarova, *Quasi-Gas Dynamic Equations*, Springer, 2009.
- [16] Yu.V. Sheretov, Dynamics of continuous media under spatiotemporal averaging, *SPC Regular and Chaotic Dynamics: Moscow-Izhevsk*, 2009.
- [17] T.G. Elizarova, Yu.V. Sheretov, Theoretical and numerical analysis of quasi-gasdynamic and quasi-fluid-dynamic equations, *Comput. Math. Math. Phys.* 41 (2001) 219–234.
- [18] T.G. Elizarova, E.V. Shil’nikov, Capabilities of a quasi-gasdynamic algorithm as applied to inviscid gas flow simulation, *Comput. Math. Math. Phys.* 49 (2009) 532–548.
- [19] T.G. Elizarova, I.A. Graur, J.-C. Lengrand, Two-fluid computational model for a binary gas mixture, *Eur. J. Mech. B Fluids* 3 (2001) 351–369.
- [20] B. Mate, I.A. Graur, T. Elizarova, I. Chirokov, G. Tejada, J.M. Fernandez, S. Montero, Experimental and numerical investigation of an axisymmetric supersonic jet, *J. Fluid Mech.* 426 (2001) 177–197.
- [21] I.A. Graur, T.G. Elizarova, A. Ramos, G. Tejada, J.M. Fernandez, S. Montero, A study of shock waves in expanding flows on the basis of spectroscopic experiments and quasi-gasdynamic equations, *J. Fluid Mech.* 504 (2004) 239–270.
- [22] A. Chpoun, T.G. Elizarova, I.A. Graur, J.C. Lengrand, Simulation of the rarefied gas flow around a perpendicular disk, *Eur. J. Mech. B Fluids* 24 (2005) 457–467.
- [23] T.G. Elizarova, A.A. Khokhlov, Yu.V. Sheretov, Quasi-gasdynamic numerical algorithm for gas flow simulations, *Int. J. Numer. Methods Fluids* 56 (2008) 1209–1215.
- [24] T.G. Elizarova, Yu.V. Sheretov, Analyse du probleme de l’écoulement gazeux dans les microcanaux par les equations quasi hydrodynamiques, *Houille Blanche. Rev. Int. Eau* 5 (2003) 66–72. Was also published in: *Congres Societe Hydrotechnique de France (SHF) “Microfluidique”*, Toulouse (2002) 309–318.
- [25] I.A. Shirokov, T.G. Elizarova, Simulation of laminar–turbulent transition in compressible Taylor–Green flow basing on quasi-gas dynamic equations, *J. Turbul.* 15 (10) (2014) 707–730.
- [26] T.G. Elizarova, V.V. Seregin, Filtered simulation method for turbulent heat and mass transfer in gas dynamic flows, in: K. Hanjalic, Y. Nagano, S. Jakirlic (Eds.), *Proceedings of the 6th International Symposium on Turbulence, Heat and Mass Transfer*, Begell House Inc., Rome, 2009, pp. 383–386.
- [27] A.A. Zlotnik, Quasi-gasdynamic system of equations with general equations of state, *Dokl. Math.* 81 (2) (2010) 312–316.
- [28] A. Zlotnik, V. Gavrilin, On quasi-gasdynamic system of equations with general equations of state and its application, *Math. Model. Anal.* 16 (4) (2011) 509–526.
- [29] A.A. Zlotnik, B.N. Chetverushkin, Parabolicity of the quasi-gasdynamic system of equations, its hyperbolic second-order modification, and the stability of small perturbations for them, *Comput. Math. Math. Phys.* 48 (2008) 420–446.
- [30] A.A. Zlotnik, Linearized stability of equilibrium solutions to the quasigasdynamic system of equations, *Dokl. Math.* 82 (2) (2010) 811–815.
- [31] T.G. Elizarova, I.S. Kalachinskaya, Yu.V. Sheretov, I.A. Shirokov, Numerical simulation of electrically conducting liquid flows in an external magnetic field, *J. Commun. Technol. Electron.* 50 (2) (2005) 227–233.
- [32] T.G. Elizarova, S.D. Ustyugov, Quasi-gas dynamic algorithm of solution of magnetohydrodynamic equations. One dimensional case, Preprint of Keldysh Institute of Applied Mathematics 1 (2011) 24 pages (in Russian) <http://library.keldysh.ru/preprint.asp?id=2011-1>.
- [33] T.G. Elizarova, S.D. Ustyugov, Quasi-gas dynamic algorithm of solution of magnetohydrodynamic equations. Multidimensional case, Preprint of Keldysh Institute of Applied Mathematics 30 (2011) 20 pages (in Russian) <http://library.keldysh.ru/preprint.asp?id=2011-30>.
- [34] T.G. Elizarova, Time averaging as an approximate technique for constructing quasi-gasdynamic and quasi-hydrodynamic equations, *Comput. Math. Math. Phys.* 51 (2011) 1973–1982.
- [35] B. Ducomet, A. Zlotnik, On a regularization of the magnetic gas dynamics system of equations, *Kinet. Relat. Model.* 6 (2013) 533–543.
- [36] T.A. Gardiner, J.M. Stone, An unsplit Godunov method for ideal MHD via constrained transport, *J. Comput. Phys.* 205 (2005) 509–539.
- [37] M. Bird, *Molecular Gas Dynamics and the Direct Simulation of Gas Flows*, Clarendon Press, Oxford, 1994.
- [38] T.A. Gardiner, J.M. Stone, An unsplit Godunov method for ideal MHD via constrained transport in three dimensions, *J. Comput. Phys.* 227 (2008) 4123.
- [39] A.A. Sukhomozgiy, Yu.V. Sheretov, Testing new algorithm of calculation one-dimensional non-stationary fluid flows with free boundary, *Bull. Tver State Univ. Ser. Appl. Math.* 4 (2012) 47–64 (in Russian).
- [40] R.-L. Jiang, C. Fang, P.-F. Chen, A new MHD code with adaptive mesh refinement and parallelization for astrophysics, *Comput. Phys. Commun.* 183 (2012) 1617–1633.
- [41] P.A. Sturrock, *Plasma Physics: An Introduction to The Theory of Astrophysical, Geophysical, and Laboratory Plasmas*, Cambridge University Press, 1994.
- [42] D.S. Balsara, Total variation diminishing scheme for adiabatic and isothermal magnetohydrodynamics, *Astrophys. J. Suppl. Ser.* 116 (1998) 133–153.
- [43] G. Tóth, The $\nabla \cdot \mathbf{B} = 0$ constraint in shock-capturing magnetohydrodynamics codes, *J. Comput. Phys.* 161 (2000) 605–652.
- [44] S.A. Orszag, C.-M. Tang, Small-scale structure of two-dimensional magnetohydrodynamic turbulence, *J. Fluid Mech.* 90 (1979) 129–143.
- [45] P. Arminjon, R. Touma, Central finite volume methods with constrained transport divergence treatment for ideal MHD, *J. Comput. Phys.* 204 (2005) 737–759.
- [46] A. Pouquet, P.D. Mininni, The interplay between helicity and rotation in turbulence: implications for scaling laws and small-scale dynamics, *Philos. Trans. R. Soc. A* 368 (2010) 1635–1662.
- [47] R.W.C.P. Versteappen, A.E.P. Veldman, Symmetry-preserving discretization of turbulent flow, *J. Comput. Phys.* 187 (2003) 343–368.
- [48] W. Dai, P. Woodward, A simple finite difference scheme for multidimensional magnetohydrodynamical equations, *J. Comput. Phys.* 142 (1998) 331–369.